Mechanical tissue optical clearing devices: evaluation of enhanced light penetration in skin using optical coherence tomography

Christopher Drew
Virginia Tech
Mechanical Engineering
MC-0298 ICTAS Building
Stanger Street, Room 325
Blacksburg, Virginia 24061

Thomas E. Milner
University of Texas at Austin
Biomedical Engineering
1 University Station, C0800
Austin, Texas 78712

Christopher G. Rylander
Virginia Tech
Mechanical Engineering, Biomedical Engineering
    and Sciences
MC-0298 ICTAS Building
Stanger Street, Room 325
Blacksburg, Virginia 24061

Abstract. We report results of a study to evaluate effectiveness of a mechanical tissue optical clearing device (TOCD) using optical coherence tomography (OCT). The TOCD uses a pin array and vacuum pressure source to compress localized regions of the skin surface. OCT images (850 and 1310 nm) of *in vivo* human skin indicate application of the TOCD provides an up to threefold increased light penetration depth at spatial positions correlated with pin indentations. Increased contrast of the epidermal–dermal junction in OCT images spatially correlates with indented zones. OCT M-scans recorded while applying the TOCD indicate optical penetration depth monotonically increased, with most improvement at early times (5 to 10 s) of TOCD vacuum application. OCT M-scans of *ex vivo* porcine skin compressed using the TOCD suggest average group refractive index of the tissue increased, corresponding to a decrease in water concentration. Results of our study indicate that mechanical optical clearing of skin may provide an effective and efficient means to deliver increased light fluence to dermal and subdermal regions. © *2009 Society of Photo-Optical Instrumentation Engineers.* [DOI: 10.1117/1.3268441]

1 Introduction

Tissue optical clearing is a research area that investigates reversibly altering light scattering within naturally turbid tissues, permitting delivery of near-collimated light deeper into tissue, and therefore potentially improving the capabilities of various optical diagnostic and therapeutic techniques. The response of tissue to application of agents such as glycerol, dimethyl sulfoxide, and related chemical species is a reduction in light scattering and corresponding increase in optical clarity. Numerous scientific and engineering publications report methods, applications, and potential mechanisms of tissue optical clearing using hyperosmotic agents.[1–7] Previous studies suggest that optical clearing of tissue using hyperosmotic agents may occur in part due to the mechanism of dehydration.

Because dehydration is an important candidate mechanism of optical clearing, we hypothesize that alternative nonchemical techniques that displace water in tissue (e.g., mechanical force) can also reduce light scattering within naturally turbid tissues. To test this hypothesis, we designed two tissue optical clearing devices (TOCDs) consisting of an array of pins that induce spatially localized tissue compression utilizing a 750-mm Hg vacuum pressure source. Optical coherence tomography (OCT) imaging was used to test the hypothesis that tissue compression will displace water underlying the pins, reduce tissue scattering, and permit delivery of increased light fluence in deep tissue regions.

Mechanical compression using a TOCD can provide several potential benefits for optical diagnostic and therapeutic techniques compared to clearing methods using chemical agents. Mechanical compression using a TOCD is less invasive and therefore safer, since no chemical agents are introduced into the tissue and the *stratum corneum* barrier function is preserved. TOCD may also provide a faster onset, more controllable, and repeatable optical clearing method. Additionally, a TOCD may have a simpler regulatory pathway, be easier to use clinically, and provide superior performance compared to chemical methods.

2 Materials and Methods

2.1 *Tissue Optical Clearing Devices* (*TOCDs*)

Two tissue optical clearing devices (TOCDs) were designed, constructed, and utilized to test our hypothesis that mechanical force can displace water and reduce light scattering within

Address all correspondence to: Christopher G. Rylander, Virginia Tech, Mechanical Engineering, Biomedical Engineering and Sciences, MC-0298 ICTAS Building, Stanger Street, Room 325, Blacksburg, Virginia 24061. Tel: 540-231-0964; Fax: 540-231-0970; E-mail: cgr@vt.edu.
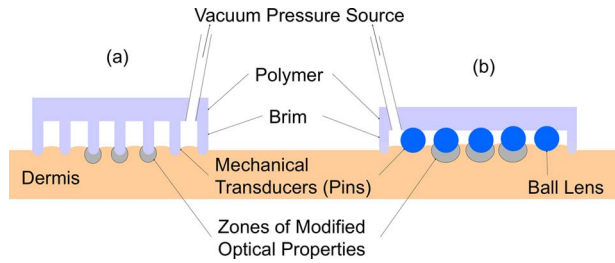
Fig. 1 Simplified cross-sectional schematic diagram of (a) first and (b) second TOCDs applied to skin.

naturally turbid tissues. The first device was designed for recording photographic and OCT images of *in vivo* human skin during TOCD application. The second device was designed for infrared imaging radiometry (IIR) studies of subdermal regions of *ex vivo* porcine skin specimens during laser irradiation of the epidermal surface during TOCD application. Photographic observations and IIR experimental results have been reported previously.[8]

The first TOCD consists of a monolithic array of pins, circumscribing brim, and vacuum pressure source [Fig. 1(a)]. The pin array, which comprises the inner chamber surface, is constructed of a translucent photoresin and transduces mechanical force to a target skin region. Pin parameters include diameter (1 mm), length (4 mm), lattice geometry (square), packing density (20% fill factor), and tip geometry (hemispherical). The TOCD brim interfaces with the tissue and forms an airtight seal when a vacuum pump (~750 mm Hg) is connected to the TOCD. Application of vacuum pressure to the chamber provides a mechanical transduction force on the tissue, causing stretching and compression of tissue between and underneath the pins, respectively. The resulting compression force provided by the pins on the tissue is equal in magnitude and opposite in direction to the load imposed by the vacuum.

The second TOCD consists of an array of 68, 3-mm-diam ball lenses arranged in a hexagonal pattern with a 50% fill factor [Fig. 1(b)]. This device incorporates radiant filters (i.e., ball lenses) to permit spatial and angular control (focusing or divergence) of radiant energy incident on the tissue. Each ball lens is epoxy-bonded to a spherically recessed cavity in a polymer plate.

2.2 Tissue Specimens

In vivo human skin was chosen for nondestructive experimentation due to its clinical significance. *In vivo* volar forearm skin of a Caucasian male volunteer (28 years, Fitzpatrick skin type III) was utilized for OCT imaging experiments. *Ex vivo* porcine skin specimens (abdomen, $n=5$) used for refractive index and thickness experiments were obtained from a local abattoir and stored at $5\,°C$ until experiments were performed.

2.3 OCT Imaging on In Vivo Skin

The first TOCD was applied with vacuum to *in vivo* human skin for 30 s and then removed. OCT (850 nm) B-scan images of the skin were recorded after device removal. Specifications of the OCT system utilized to record the B-scan images have been reported previously.[9]

OCT M-scan images permit visualization of time- and depth-resolved changes in the tissue backreflectance at a single lateral position. OCT M-scan images were acquired with light propagating through a single pin of the first TOCD while applied to *in vivo* human skin. Volar forearm skin was brought into contact with the first TOCD for 2 s before time-resolved OCT images were acquired. Five seconds after beginning the OCT M-scan image acquisition, the vacuum was activated, inducing tissue compression beneath the pins of the TOCD. Vacuum application and OCT M-scan image acquisition continued for 25 s.

The second TOCD prototype was applied with vacuum to *in vivo* human skin for 30 s and then removed. A swept-source OCT (1310-nm wavelength) system utilizing a tunable laser source (Santec HSL-2000; Ohkusa, Japan) was utilized to record B-scan images (20 Hz, 1000 A-lines) of the skin after device removal. Specifications of a similar swept-source OCT system have been reported previously.[10]

2.4 OCT Imaging to Determine Refractive Index and Thickness of Ex Vivo Porcine Skin

The second TOCD prototype was applied to *ex vivo* porcine skin for a period of 18 s. The 750-mm Hg vacuum pressure source was activated after 4 s of data acquisition, causing compression of the tissue by the ball lenses. OCT images were acquired through the skin specimens, permitting identification of the top and bottom skin surfaces and the crown of the ball lens.

Optical path lengths determined by OCT A-scans revealed the time-dependent refractive index and thickness of the skin sample in response to TOCD application. At a single *x* coordinate corresponding to the crown of the ball lens, optical path length *y* coordinate was measured corresponding with the top of the skin (y_{top}), the bottom of the skin (y_{bottom}), and the top of the ball lens (y_{lens}) as a function of time. The skin position at the crown of the ball lens was chosen for analysis because the largest overall force applied to the tissue and therefore greatest water transport and thinning is expected at this position. Physical thickness and group refractive index of the sample was calculated from measured optical path lengths according to Eqs. (1) and (2)[11]:

$$thickness(t) = [y_{bottom}(t) - y_{top}(t)] - [y_{lens}(t) - y_{lens}(0)].$$
(1)

The group index is found by

$$n_g(t) = \frac{[y_{bottom}(t) - y_{top}(t)]}{thickness(t)}.$$
(2)

In Eq. (1), t denotes time since the experiment began, and $y_{lens}(t=0)$ is the original path length to the ball lens before tissue is placed above it.

2.5 Water Content Determination of Ex Vivo Skin

Biphasic mixture approaches have been developed extensively to describe the properties of biological tissues, including skin.[12,13] Proteinaceous structures including collagen, cell membranes, and cellular organelles make up the majority of the solid phase of skin and have a refractive index of 1.43 to
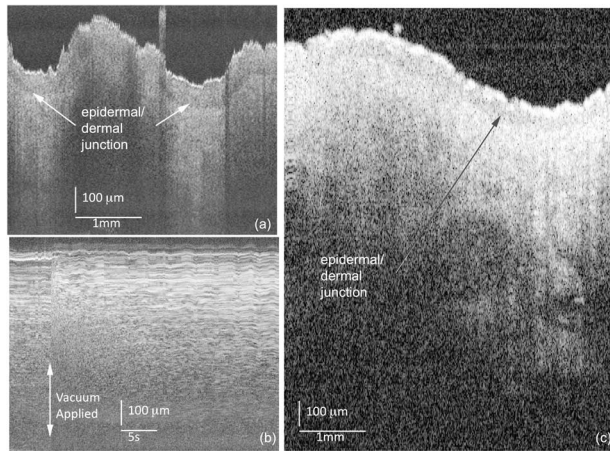
Fig. 2 *In vivo* human skin: (a) OCT B-scan image (850 nm) following application of the first TOCD. (b) OCT M-scan image (1310 nm) before and during application of the first TOCD. (c) OCT B-scan image (1310 nm) following application and removal of the second TOCD.

Fig. 3 OCT B-scan image of porcine skin and TOCD ball lens (a) prior to vacuum application and (b) during vacuum application. See text for description of red vertical line. (Color online only.)

1.53 (Ref. 14). Noting that skin is principally composed of water ($\sim 70\%$), we utilize a biphasic model of skin consisting of a mixture of low refractive index water ($n = 1.33$) and high refractive index dry protein ($n = 1.53$). Following this assumption, the Lorentz-Lorenz rule of mixtures can be used to relate measured refractive index of skin, n_{skin}, to its chemical composition (water and protein volume fraction, Φ_{H_2O} and Φ_P), as shown in Eq. (3):[15]

$$\frac{(n_{skin}^2 - 1)}{(n_{skin}^2 + 2)} = \frac{(n_{H_2O}^2 - 1)}{(n_{H_2O}^2 + 2)}\Phi_{H_2O} + \frac{(n_P^2 - 1)}{(n_P^2 + 2)}\Phi_P, \qquad (3)$$

where n_{skin}, n_{H_2O}, and n_P are the refractive indices of skin, water, and protein, respectively. Assuming that skin is a fully saturated medium, the volume fractions of the water and protein are related by

$$\Phi_{H_2O} + \Phi_P = 1. \qquad (4)$$

OCT images can be analyzed to provide water content as a function of time (t) and lateral (x) position so that water transport can be deduced from the recorded spatiotemporal data. A limitation of this technique is that because measured refractive index is an average across the full thickness of the skin specimen, the measurement is insensitive to water concentration gradients in depth (y coordinate). The limitation is not expected to be severe, since water concentration in skin varies primarily in the *stratum corneum* and is constant in the lower portions of the epidermis and throughout the dermis.[16]

3 Results

3.1 *In Vivo OCT Images*

Recorded OCT images [Fig. 2(a); 850 nm] after removal of the first TOCD revealed large contrast differences between tissue regions directly below and adjacent to pin indentations. Regions of increased light penetration were observed to correlate directly with skin indentations produced by TOCD pins. Light penetration depth under the pins is enhanced two- to
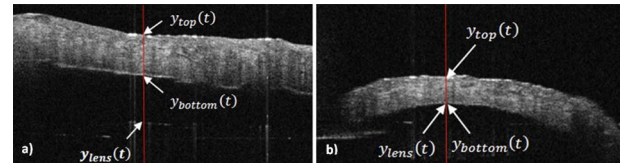
threefold over peripheral tissue regions. Penetration depth in this study was defined as the optical depth from the surface of the tissue vertically downward to the background noise level at each lateral position in each OCT image. Increased OCT image contrast of the epidermal–dermal junction is observed in regions indented by the TOCD pins. Native *in vivo* human volar forearm skin has a characteristic smooth surface. After TOCD application and removal, indentations approximately 200 μm deep were observed on the skin surface corresponding with pin positions.

OCT M-scan images [Fig. 2(b); 1310 nm] recorded before and during vacuum activation of the first TOCD indicate vacuum activation was accompanied by an abrupt decrease in both amplitude of surface reflection and epidermal thickness. Backreflectance from superficial depths (100 to 200 μm) is noticeably increased immediately after vacuum application. Additionally, backreflectance increases from deeper positions (> 200 μm) throughout the dermis. Optical penetration depth continued to increase monotonically throughout the entire image acquisition period, with most improvement at early times (5 to 10 s) after TOCD vacuum application.

OCT B-scan [Fig. 2(c); 1310 nm] images recorded following application and removal of the second TOCD revealed a distinction between tissue regions directly below and adjacent to pin indentations. Regions of increased light penetration were observed to correlate directly with skin indentations produced by the pins. Increased OCT image contrast of the epidermal–dermal junction is observed in compressed regions directly below the TOCD pins.

3.2 *Refractive Index, Thickness, and Water Content Measurements of Ex Vivo Skin*

OCT images recorded through application of the second TOCD prior to [Fig. 3(a)] and during [Fig. 3(b)] vacuum application revealed a noticeable change in tissue thickness. Vacuum-induced tissue compression induced a 37% decrease in thickness (from 0.67 mm to 0.41 mm). Figure 4 shows porcine skin thickness, refractive index, and water volume fraction over the 18-s duration of the experiment. Prior to vacuum-induced stretching and compression, the mean group index of the skin was 1.38, which is comparable to values found in the literature.[17] During vacuum application, skin's mean group index increased nearly 8% to 1.46. Using the Lorentz-Lorenz equation and our assumption of a protein–water biphasic mixture for skin, the measured change in tissue refractive index corresponds to a decrease in water volume fraction from approximately 0.7 (70%) before TOCD application to 0.3 (30%) after TOCD application.
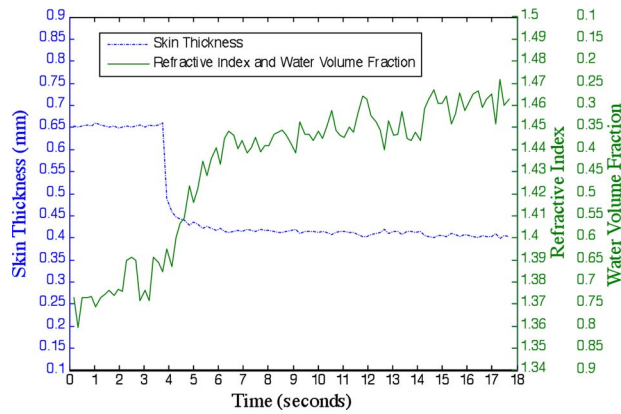
Fig. 4 Skin thickness, mean group index, and water volume fraction versus time. Vacuum was applied to porcine skin after 4 s and continued through the 18-s time duration.

4 Discussion

4.1 Skin Water Content

A natural gradient of water content as a function of depth exists in skin. At the *stratum corneum*, the outermost layer of epidermis, water content depends on atmospheric humidity and may be as low as 15% (Ref. 18). At a depth of about 50 μm, near the epidermal–dermal junction, the water content is about 70% and remains constant throughout the dermis. Water and blood, having a relatively high permeability, are likely constituents to be displaced from regions below the pins due to TOCD application. Increased tissue volume surrounding the pins (vacuum-stretched-tissue regions) provides additional storage capacity for displaced water and blood.

4.2 OCT Imaging

OCT is an imaging technique capable of measuring backreflected light intensity as a function of optical depth (path length) in a scattering tissue specimen. Optical path length is the product of physical path length and group refractive index. *In vivo* OCT images were displayed with respect to physical path length (Fig. 2) by assuming a spatially and temporally uniform group refractive index for skin ($n=1.4$). This assumption is reasonable because the movement of water ($n=1.33$) does not significantly modify the refractive index distribution in skin. At 70% water fraction, the refractive index of skin is 1.38 based on the Lorentz-Lorenz model and our assumptions [Eqs. (3) and (4)]. If TOCD compression completely dehydrates skin, its index would approach that of dried protein ($n\cong1.53$). The percent error in calculating physical path length based on an unknown refractive index between these extreme limiting cases (1.38 to 1.53) is less than 10%.

Recorded OCT images demonstrated increased backreflectance at all depths in skin beneath regions compressed by TOCD pins. Consequently, light penetration depth under the pins is enhanced over peripheral tissue regions approximately threefold at 850 nm [Fig. 2(a)] and twofold at 1310 nm [Fig. 2(c)]. Increased light penetration depth is primarily due to reduced optical scattering in the tissue; the result of increased refractive index will have a minor contribution $<10\%$, as described earlier. Greater improvement in penetration depth at

850 nm compared to 1310 nm may be understood in part because light scattering in tissue is greater at shorter wavelengths (850 nm) and changes induced at shorter wavelengths by water displacement are proportionately greater. Variation between TOCD devices also may contribute to the observed variation in optical penetration depth.

At tissue depths greater than 100 μm, light collected by OCT has forward-scattered multiple times and backreflected once. Attenuation in OCT signal versus depth is dominated by an increasing number of forward-scattering events, causing light to deviate at high angles from the incident direction and preventing OCT collection of single backscattering events. The decrease in OCT signal amplitude with increasing tissue depth is not believed to be due to a reduction in probability of single backscattering (which is only a function of tissue structure and refractive index). Increased backreflectance observed below the TOCD pins in the recorded OCT images is interpreted as an intrinsic reduction in light scattering. More light reaches each tissue depth because less light is lost to higher-angle scattering. Dehydration likely decreases the reduced scattering coefficient of the skin, which may be caused by a reduction in the number of scattering events per unit length (μ_s) or an increase in the anisotropy factor, g, which is the average cosine of the angle of scattering. As g approaches unity, light becomes more forward-scattering. Determining the relative contribution of a reduced scattering coefficient and increased anisotropy factor will require further experimentation.

To permit dynamic measurement of the *ex vivo* tissue group refractive index during compression, the technique of Sorin and Gray was utilized. Dynamic water content was then determined using Lorentz-Lorenz rules for a biphasic mixture. The initial *ex vivo* skin water content ($\sim70\%$), determined from the OCT measurement and Eqs. (4) and (5), matches values measured using alternative techniques such as magnetic resonance chemical shift microimaging.[19] Because 15 to 90% of tissue water is believed to be tightly bound to proteins such as collagen,[20,21] full dehydration of skin cannot be realized through application of mechanical forces. The residual water content (30%) measured after TOCD application is consistent with residual water that is tightly bound to collagen and other proteins in the dermis.

4.3 Relationship between Water Content and Light Scattering in Tissue

Skin acts as a highly scattering medium for visible to near-infrared (NIR) wavelengths due to its complex and inhomogeneous morphological structure. Light scattering in biological tissues is caused primarily by spatial variation in electronic polarizability at optical frequencies, which may be characterized by the optical index of refraction, n. Light scattering theories such as Mie and Rayleigh-Gans predict reduced scattering cross sections [$\sigma_s'(\text{cm}^2)$] for a single particle as a function of scattering particle radius and refractive index, surrounding medium refractive index, and vacuum wavelength of light.[1,22] For a dense distribution of scattering particles, reduced scattering coefficient [$\mu_s'(\text{cm}^{-1})$] is related to the reduced scattering cross section by a simple heuristic particle-interaction model:

$$\mu'_s = \frac{\phi(1-\phi)}{V}\sigma'_s, \qquad (5)$$

where ϕ is volume fraction of scattering particles, and V is the volume of a single scattering particle. Parabolic dependence on ϕ was first introduced by Twersky[23] and ensures that the reduced scattering coefficient is zero in the limits of null ($\phi=0$) or unity ($\phi=1$) volume fractions. As the fractional volume of scattering particles approaches unity, the scatterer represents less of an optical discontinuity in its environment. The heuristic particle-interaction model predicts that maximum scattering occurs for a scattering particle volume fraction equal to 0.5 (Refs. 24 and 25).

Equation (5) is useful for evaluating potential mechanisms involved in mechanical optical clearing. The parabolic dependence of μ'_s on ϕ can predict the effect of water displacement that modifies the scattering particle packing density. Several investigators have suggested that dehydration alone can reduce scattering in soft tissue by displacing water from the space between collagen fibrils, increasing protein and sugar concentrations, and decreasing refractive index mismatch.[26–30] Refractive index matching and shape/structural changes to individual scattering particles affect the reduced scattering cross section (σ'_s). Water movement resulting from mechanical compression may reduce light scattering by (1) increasing the volume fraction of scattering particles (i.e., collagen fibers, cell organelles) past or beyond 0.5 toward unity; and (2) intrinsic refractive index matching due to increased proteoglycan concentration in ground substance. Both parameters may experience a transient excursion dependent on applied compressive stress and water transport kinetics within tissue.

Localized mechanical compression in tissue may modify the absorption coefficient through displacement of light-absorbing chromophores such as water and blood. Reduced blood volume in tissue will decrease light absorption by hemoglobin, therefore increasing light penetration depth. The decreased blood perfusion in compressed tissue regions will reduce the ability of the tissue to naturally rehydrate through the mechanism of osmotic flow of water from vascular to intracellular and interstitial compartments. Additionally, mechanical compression may reduce the physical path length between the tissue surface and a physiological target, thereby improving radiant throughput. Modified optical properties and tissue thickness may increase fluence at deep-targeted chromophores, potentially improving optical imaging and therapeutic procedures (Fig. 5). Measurements of the change in absorption coefficient, scattering coefficient, and thickness as a function of tissue depth and time are required for evaluating the relative contribution of each to increased fluence.

5 Conclusions

Results of our study suggest that mechanical optical clearing can laterally displace interstitial water and blood below TOCD pins, reducing tissue thickness, and modifying the group refractive index. The increase in group refractive index observed in *ex vivo* porcine skin is believed to possibly modify optical properties. OCT B-scan and M-scan images reveal an intrinsic increase in light penetration depth underneath the pins compared to surrounding regions. The scattering coefficient may be locally reduced by increased scattering
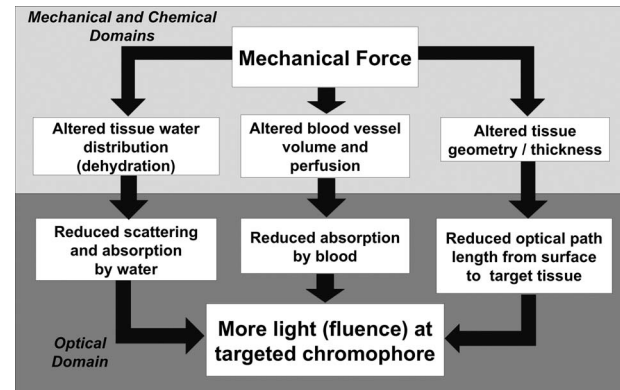

Fig. 5 Potential pathways for increasing fluence at deep targeted chromophores using mechanical force.

particle density and increased proteoglycan concentration in ground substance causing greater intrinsic refractive index matching.

References

1. H. Liu, B. Beauvoit, M. Kimura, and B. Chance, "Dependence of tissue optical properties on solute-induced changes in refractive index and osmolarity," *J. Biomed. Opt.* **1**(2), 200–211 (1996).
2. V. V. Tuchin, I. L. Maksimova, D. A. Zimnyakov, I. L. Kon, A. H. Mavlutov, and A. A. Mishin, "Light propagation in tissues with controlled optical properties," *J. Biomed. Opt.* **2**, 401–417 (1997).
3. G. Vargas, E. K. Chan, J. K. Barton, H. G. Rylander III, and A. J. Welch, "Use of an agent to reduce scattering in skin," *Lasers Surg. Med.* **24**, 133–141 (1999).
4. R. K. Wang and X. Xu, "Concurrent enhancement of imaging depth and contrast for optical coherence tomography by hyperosmotic agents," *J. Opt. Soc. Am. B* **18**(7), 948–953 (2001).
5. A. T. Yeh, B. Choi, J. S. Nelson, and B. J. Tromberg, "Reversible dissociation of collagen in tissues," *J. Invest. Dermatol.* **121**(6), 1332–1335 (2003).
6. B. Choi, L. Tsu, E. Chen, T. S. Ishak, S. M. Iskandar, S. Chess, and J. S. Nelson, "Determination of chemical agent optical clearing potential using *in vitro* human skin," *Lasers Surg. Med.* **36**, 72–75 (2005).
7. C. G. Rylander, O. F. Stumpp, T. E. Milner, N. J. Kemp, J. M. Mendenhall, K. R. Diller, and A. J. Welch, "Dehydration mechanism of optical clearing in tissue," *J. Biomed. Opt.* **11**(4), 041117-1–7 (2006).
8. C. G. Rylander, T. E. Milner, and J. S. Nelson, "Mechanical tissue optical clearing devices: enhancement of light penetration and heating of *ex vivo* porcine skin and adipose tissue," *Lasers Surg. Med.* **40**(10), 688–694 (2008).

9. N. J. Kemp, J. Park, H. N. Zaatari, H. G. Rylander III, and T. E. Milner, "High-sensitivity determination of birefringence in turbid media with enhanced polarization-sensitive optical coherence tomography," *J. Opt. Soc. Am. A* **22**, 552–560 (2005).

10. R. Huber, M. Wojtkowski, J. G. Fujimoto, J. Y. Jiang, and A. E. Cable, "Three-dimensional and C-mode OCT imaging with a compact, frequency swept laser source at 1300 nm," *Opt. Express* **13**(26), 10523–10538 (2005).

11. W. V. Sorin and D. F. Gray, "Simultaneous thickness and group index measurement using optical low-coherence reflectometry," *IEEE Photonics Technol. Lett.* **4**(1), 105–107 (1992).

12. V. C. Mow, S. C. Kuei, W. M. Iai, and C. G. Armstrong, "Biphasic creep and stress-relaxation of articular-cartilage in compression—theory and experiments," *ASME J. Biomech. Eng.* **102**(1), 73–84 (1980).

13. C. W. J. Oomens, D. H. Vancampen, and H. J. Grootenboer, "A mixture approach to the mechanics of skin," *J. Biomech.* **20**(9), 877–885 (1987).

14. X. Wang, T. E. Milner, M. C. Chang, and J. S. Nelson, "Group refractive index measurement of dry and hydrated type I collagen films using optical low-coherence reflectometry," *J. Biomed. Opt.* **1**(2), 212–216 (1996).

15. W. Heller, "Remarks on refractive index mixture rules," *J. Phys. Chem.* **69**(5), 1123–1129 (1965).

16. P. J. Caspers, G. W. Lucassen, E. A. Carter, H. A. Bruining, and G. J. Puppels, "*In vivo* confocal Raman microspectroscopy of the skin: noninvasive determination of molecular concentration profiles," *J. Invest. Dermatol.* **116**(3), 434–442 (2001).

17. G. J. Tearney, M. E. Brezinski, J. F. Southers, B. E. Bouma, M. R. Hee, and J. G. Fujimoto, "Determination of the refractive index of highly scattering human tissue by optical coherence tomography," *Opt. Lett.* **20**(21), 2258–2260 (1995).

18. I. H. Blank, "Factors which influence the water content of the *stratum corneum*," *J. Invest. Dermatol.* **18**, 433–440 (1952).

19. A. C. Wright, D. E. Bohning, A. P. Pecheny, and K. M. Spicer, "Magnetic resonance chemical shift microimaging of aging human skin *in vivo*: initial findings," *Skin Res. Technol.* **4**, 55–62 (1998).

20. S. Naito, M. Hoshi, and S. Mashimo, "*In vivo* dielectric analysis of free water content of biomaterials by time domain reflectometry," *Anal. Chem.* **251**, 163–172 (1997).

21. M. Gniadecka, O. F. Nielsen, D. H. Christensen, and H. C. Wulf, "Structure of water, proteins, and lipids in intact human skin, hair, and nail," *J. Invest. Dermatol.* **110**, 393–398 (1998).

22. R. Graaff, J. G. Aarnoudse, J. R. Zijp, P. M. A. Sloot, F. F. M. de Mul, J. Greve, and M. H. Koelink, "Reduced light-scattering properties for mixtures of spherical particles: a simple approximation derived from Mie calculations," *Appl. Opt.* **31**(10), 1370–1376 (1992).

23. V. Twersky, "On scattering of waves by random distributions. II. Two-space scatterer formalism," *J. Math. Phys.* **3**(4), 724–734 (1962).

24. A. Ishimaru, *Wave Propagation and Scattering in Random Media*, Academic Press, San Diego, CA (1978).

25. S. Fraden and G. Maret, "Multiple light scattering from concentrated, interacting suspensions," *Phys. Rev. Lett.* **65**(4), 512–515 (1990).

26. G. A. Askar'yan, "The increasing of laser and other radiation transport through soft turbid physical and biological media," *Sov. J. Quantum Electron.* **9**(7), 1379–1383 (1982).

27. A. P. Ivanov, S. A. Makarevich, and A. Ya. Khairulina, "Propagation of radiation in tissues and liquids with densely packed scatterers," *J. Appl. Spectrosc.* **47**, 662–668 (1988).

28. P. Rol, P. Neiderer, U. Durr, P. D. Henchoz, and F. Frankhauser, "Experimental investigation on the light scattering properties of the human sclera," *Ophthalmic Surg. Lasers* **3**, 201–212 (1990).

29. E. K. Chan, B. Sorg, D. Protsenko, M. O'Neil, M. Motamedi, and A. J. Welch, "Effects of compression on soft tissue optical properties," *IEEE J. Sel. Top. Quantum Electron.* **2**(4), 943–950 (1996).

30. H. Shangguan, S. A. Prahl, S. L. Jacques, and L. W. Casperson, "Pressure effects on soft tissues monitored by changes in tissue optical properties," *Proc. SPIE* **3254**, 366–371 (1998).